HOSTED BY
ELSEVIER
Available online at www.sciencedirect.com
ScienceDirect
Soils and Foundations 64 (2024) 101522
www.elsevier.com/locate/sandf

Technical Paper

Evaluation of the damping ratio of compacted sodium and calcium bentonites in unsaturated conditions

X. Pintado [a], S. Kumpulainen [a], E. Romero [b,c], J. Suriol [b], A. Lloret [b], R.C. Weber [d], B.N. Madhusudhan [e], A. Ferrari [f,g,*], J. Kim [f], K. Koskinen [h], V. Heino [h]

[a] *Mitta Engineering Oy, Vantaa, Finland*
[b] *Department of Civil and Environmental Engineering, Universitat Politècnica de Catalunya (UPC), Barcelona, Spain*
[c] *International Centre for Numerical Methods in Engineering (CIMNE), Geomechanics Group, Barcelona, Spain*
[d] *Universidade do Vale do Taquari (Univates), Brazil*
[e] *Department of Engineering and the Environment. University of Southampton (Soton), United Kingdom*
[f] *Laboratory for Soil Mechanics, École Polytechnique Fédérale de Lausanne (EPFL), Switzerland*
[g] *Engineering Department, Università degli Studi di Palermo, Italy*
[h] *Posiva Oy, Eurajoki, Finland*

Received 6 December 2023; received in revised form 13 September 2024; accepted 27 September 2024
Available online 17 October 2024

Abstract

Bentonites are going to be part of the Engineered Barrier System (EBS) in deep geological disposal facilities for the safe disposal of spent nuclear fuel. Some of these repositories might be constructed in tectonically active locations, and some other repository locations might have seismic risks in future related to climate changes (e.g. glaciations).

The damping ratio is one of the parameters considered in dynamic analysis, and it can be measured by different methods. In this work, the damping ratio was measured in two different bentonites with the resonant column device and in one of these bentonites, it was also measured with the hollow cylinder, simple shear and triaxial tests in unloading–reloading paths. The results are presented in Pintado et al. (2019; 2023). The tests were carried out at different laboratories.

The samples were compacted at different dry densities and degrees of saturation and tested with different confinement pressures and strain levels to study the influence of the shear strain, degree of saturation, dry density and confinement pressure and also the influence of the test method. The two studied bentonites had different plasticity indices which was also considered in the analysis.

The results showed a clear dependence of the damping ratio on the confinement pressure and the shear strain but not as clear on the degree of saturation, the dry density and the plasticity index. The damping ratio measured by the hollow cylinder test followed the tendency of the resonant column results. The triaxial test presented larger values of damping ratios than following the tendency of the hollow cylinder and resonant column tests. The simple shear test did not follow the tendency of the other tests, presenting lower damping ratio values. All tests presented large scatter.

Keywords: Resonant column test; Hollow cylinder test; Triaxial test; Engineered barrier system; Simple shear test; Damping ratio

1. Introduction

Deep geological disposal is one of the options for the long-term storage of the spent nuclear fuel generated in nuclear power plants in many countries. Some of these

* Corresponding author at: Laboratory for Soil Mechanics, École Polytechnique Fédérale de Lausanne (EPFL), Switzerland.
E-mail address: alessio.ferrari@epfl.ch (A. Ferrari).

https://doi.org/10.1016/j.sandf.2024.101522
0038-0806/

countries are located on active plate margins like Japan (Apted et al. 2004; NUMO, 2017) and Taiwan (Peng, 2013; Hung et al. 2020) or have considered to construct the repository near active plate margins, like the United States in Yucca Mountain (Stepp et al. 2001). In such places, the dynamic loads due to earthquakes should be considered when the bentonite is still in unsaturated conditions. Other countries far from active plates, like Finland and Sweden, might have large earthquakes at the time of ice-sheet retreat during future glacial periods (Saari, 2012; Posiva, 2013, Winberry et al. 2020; Lei and Loew, 2021), meaning that the dynamic analysis should not be totally excluded in these places either; in this setting, this analysis is related to long term performance and should be carried out in saturated conditions. Further, during the construction phase of the deep geological repository deposition tunnels and deposition holes, microseismicity from construction (Kaisko and Malm, 2019; Kuusisto et al. 2023) might also affect the engineered barriers already constructed that are still in unsaturated conditions.

Part of the engineered barrier system in deep geological disposals in Sweden and Finland will be constructed with bentonites (SKB, 2010; Posiva, 2013). Bentonites are clays with high smectite content and other clay minerals as well as non-clay minerals Bentonite clays have high plasticity, low hydraulic conductivity and high swelling capacity. Studies in sodium bentonites or mixtures of sodium bentonite with other components like sand or cement have been carried out for measuring the damping ratio with different methods and under different conditions (Nakamura et al. 2009; Yang and Woods, 2015; Yang et al. 2020). Similar studies have also been performed in calcium bentonites (Balagosa et al. 2020). In particular, Tsai et al. (2019) have been performed tests in Wyoming-type bentonite measuring the damping ratio. Yang and Woods (2015), Tsai et al. (2019) and Balagosa et al. (2020) carried out resonant column tests. Nakamura et al. (2009) hollow torsional (hollow cylinder) tests and Yang et al. (2020), cyclic triaxial tests. Yang and Woods (2015) performed also ultrasounds and tests with bender elements. However, so far only a limited amount of information concerning the effects of saturation and density on the value of the damping ratio in bentonites can be found. This article presents the measured damping ratio in two bentonites; the first one is sodium bentonite (Wyoming-type bentonite), where the damping ratio was measured with the resonant column, hollow cylinder and triaxial test set-ups and the second one is calcium bentonite (FEBEX bentonite), where the damping ratio was only measured with the resonant column device. The work emphasizes on the dependency of the damping ratio on the shear strain, degree of saturation, dry density and confinement pressure. The possible dependency on the plastic index was also assessed.

The tests were carried out in unsaturated conditions under constant water content conditions (Bishop and Donald, 1961).

The resonant column tests were performed at the Technical University of Catalonia (UPC) and at the University of Southampton (Soton). These tests are presented in Pintado et al. (2019). Some unsaturated triaxial tests and the hollow cylinder tests were also carried out at the UPC. Finally, some unsaturated triaxial tests and the simple shear tests were performed at the École Polytechnique Fédérale de Lausanne (EPFL). These tests are presented in Pintado et al. (2023).

2. Materials and methods

2.1. Materials

Wyoming-type bentonites are sold under different commercial names (among which, MX-80) characterized by its high content of smectite (88 %), and a cation exchange capacity (CEC) around 0.86 eq/kg, from which most of the sites are occupied by sodium. The liquid limit is around 500 %, the plasticity index around 450 % and the specific surface area is 624 m^2/g. The density of solid particles considered is 2780 kg/m^3. More information about this material can be found in Karnland et al. (2006), Tang and Cui (2010), and Kiviranta et al. (2018).

FEBEX bentonite is also characterized for its high content of smectite, larger than 90 %, cation exchange capacity between 0.96 and 1.02 eq/kg, from which most of the sites are occupied by calcium. The limit liquid is around 102 %, the plasticity index around 53 %, and the specific surface area is 725 m^2/g. The considered density of solid particles is 2720 kg/m^3. Information about this material can be found in Villar and Lloret (2001, 2008) and Castellanos et al. (2008).

2.2. Methods

2.2.1. Sample preparation

Tests were performed in unsaturated conditions. The preparation of the samples in resonant column tests was carried out mixing powdered bentonite with deionized (DI) water (for Wyoming-type bentonite) or distilled water (for FEBEX bentonite), and in hollow cylinder tests, unsaturated triaxial tests and simple shear tests, mixing with different type of mixers, depending on the amount of soil to be prepared, or manually, powdered bentonite with saline water (10 g/L mixture of NaCl and $CaCl_2$ with Ca^{2+}/Na^+ mass ratio being 1:2) till reaching the target water content. After that, the water content was measured following the procedure indicated in ASTM D2216-19 (2019). Samples were statically compacted in oedometric conditions to dry densities between 1430 and 1750 kg/m^3 in resonant column tests, to around 1630 kg/m^3 in triaxial tests, to around 1390 kg/m^3 in hollow cylinder tests and to around 1535 kg/m^3 in simple shear tests. The target degrees of sat-

uration ranged between 10 % and 95 % in resonant column tests; 85 %, 90 % and 95 % in unsaturated triaxial tests and hollow cylinder tests and 64–74 % in simple shear tests.

Saline water was used in some tests because it is the composition of the groundwater in Olkiluoto (Ruotsalainen et al., 2000), the location where the Finnish spent nuclear fuel repository is in construction. The test set-ups were made of stainless steel or coated steel. Due to there was no water flow through the test -systems, the formation of rust was not considered to be an issue.

The difference in samples' dry density for the different type of tests was due to the compaction process, which in hollow cylinder and simple shear tests did not allow to reach higher preferred dry densities. The samples were compacted in steel moulds with pistons in both sides of the sample in order to have as much as possible uniform dry density distribution and to minimize the effect of friction between the mould and the soil during the compaction process. Table 1 and Table 2 show the properties of the samples for the resonant column tests, Table 3 summarizes the characteristics of the triaxial tests samples.

Table 4 shows the initial properties of the samples tested in hollow cylinder device and Table 5 the initial properties of the samples tested in simple shear apparatus. The tables also show the confinement pressure (axial stress in simple shear tests) applied during the tests.

The time evolutions of the vertical strain in resonant column tests were measured in all samples to control the time needed to reach the end of the consolidation period after the isotropic stress increments. The time required for the samples to consolidate varied (between 3 and 200 h) due to differences in their degree of saturation and the dry density. The evolution of volumetric strains over time resulting from isotropic stress increment in hollow cylinder and triaxial tests was monitored to assess equalization. Simple shear tests started after the stabilization of the axial strain after applying the axial stress.

2.2.2. Resonant column tests (RC)

The damping ratio of bentonite samples was determined using a Stokoe-type resonant column under torsional mode of vibration (Anderson and Stokoe, 1978). This device can measure the shear modulus (G) and the logarithmic decrement (δ) following the procedure outlined in ASTM D4015-15e1 (2015) as a function of the shear strain γ. Shear modulus measurements have been presented in Pintado et al. (2019), where it is also described the calculation of the shear strains. The isotropic confining stress (p) varied from 100 to 800 kPa for tests on FEBEX bentonite. For Wyoming-type bentonite, isotropic stresses ranged from $p = 100$ to 800 kPa in the tests performed at the UPC and from $p = 400$ to 10 000 kPa in the tests done at the Soton.

The damping can be considered as a measurement of the energy dissipation in a dynamic system. In free vibrations, it is associated to the reduction of the amplitude with the time and in forced vibrations, with the reduction of the amplitude that the system would have without damping. Usually, the damped harmonic oscillator can be simulated with a viscous damper, which produces a force in a direction to oppose the motion. This force depends on the velocity of the system. The equilibrium equation of a damped harmonic oscillator is:

$$m\frac{d^2u}{dt^2} + c\frac{du}{dt} + ku = Q_0 sin(\omega t + \varphi_0) \quad (1)$$

where m is the mass of the system, c is the damping coefficient, k the stiffness, Q_0 is the force, ω is the frequency, φ_0 the phase of the force, u the displacements and t the time. The damping coefficient is often related to the critical damping:

$$c_c = 2\sqrt{km} \quad (2)$$

The critical damping determines the behaviour of the damped harmonic oscillator: if $c < c_c$, the oscillator is

Table 1
Initial properties of the resonant column test samples in FEBEX bentonite after compaction. Tests carried out at the UPC. The confinement pressure was 100-200-400-800 kPa in all cases. Low degrees of saturation are expected close to canister at the early stages (Toprak et al. 2020).

Test	Height (mm)	Diameter (mm)	Void ratio (–)	Dry density (kg/m^3)	Water content (%)	Degree of Saturation (%)
FX1	76.0	38.0	0.63	1670	14.8	62
FX2	78.3	38.2	0.72	1580	14.7	54
FX4	79.9	38.4	0.77	1540	3.4	12
FX5	79.4	38.4	0.74	1560	2.8	10
FX6	78.5	38.3	0.68	1620	24.6	95
FX7	79.2	38.1	0.64	1660	21.3	87
FX8	79.4	38.5	0.65	1650	4.7	19
FX9	79.5	38.4	0.57	1730	9.7	45
FX10	78.5	38.4	0.64	1660	3.7	15
FX11	79.5	38.4	0.58	1720	10.4	47
FX12	78.5	38.3	0.66	1640	23.6	95
FX13	78.0	38.1	0.56	1740	10.6	49
FX14	79.0	38.4	0.62	1680	3.7	16
FX15	80.2	38.6	0.68	1620	12.7	50

Table 2
Initial properties of resonant column test samples in Wyoming-type bentonite after compaction. The confinement pressures were 100-200-400-800 kPa at the UPC tests and 400-800-2000-5000-10000 kPa at the Soton tests.

Place	Test	Height (mm)	Diameter (mm)	Void ratio (−)	Dry density (kg/m^3)	Water content (%)	Degree of Saturation (%)
UPC	P1	79.4	38.3	0.59	1750	10.7	51
	P2	72.7	38.0	0.78	1560	19.0	69
	P3	85.8	38.0	0.71	1630	19.9	77
	P4	74.0	38.0	0.72	1620	17.3	68
	P5	86.2	37.8	0.94	1430	26.1	76
	P6	75.1	37.7	0.76	1580	24.7	92
	P7	78.5	38.1	0.73	1610	15.8	60
	P8	78.6	38.1	0.70	1640	18.4	74
	P9	78.5	38.1	0.72	1620	22.3	89
	P10	78.7	37.8	0.65	1680	21.1	89
	P11	80.2	37.8	0.50	1750	26.5	96
	S1	78.3	38.0	0.73	1610	17.0	67
	S2	78.2	38.0	0.74	1600	15.5	58
	S3	78.2	38.0	0.71	1630	21.7	86
	S4	78.4	38.0	0.67	1660	15.4	63
Soton	HP1	130.0	70.0	0.64	1700	15.3	67
	HP2	131.0	70.0	0.62	1720	17.3	78
	HP3	136.0	70.0	0.60	1740	23.0	89

Table 3
Initial properties of triaxial test samples after compaction. The confinement pressure was 1600 kPa at the UPC tests and 4000 kPa at the EPFL tests.

Place	Test	Height (mm)	Diameter (mm)	Void ratio (−)	Dry density (kg/m^3)	Water content (%)	Degree of saturation (%)	Ramp[1)] (Pa/s)	*Deviator rate (Pa/s)* Axial strain rate[2)] (%/min)
UPC	TRI 1a	36.06	38.00	0.70	1631	21.5	85	22	*300*
	TRI 2a	36.06	38.00	0.71	1630	22.9	90	22	*300*
	TRI 3a	36.06	38.00	0.70	1633	23.9	95	22	*300*
EPFL	TRI 1b	102.14	50.48	0.74	1596	21.4	85	2500	0.3
	TRI 2b	101.61	50.03	0.70	1635	22.7	90	2500	0.3
	TRI 3b	101.49	50.00	0.71	1628	24.1	94	2500	0.3

[1)] Ramp of the confining pressure increment. The confining pressure was fixed till the axial displacements were stabilized.
[2)] Deviator rates and axial strain rates are provided in *italic* and in regular font style, respectively.

Table 4
Characteristics of the tests performed in the hollow cylinder apparatus. Tests carried out at the UPC.

Test	Void ratio (−)	Dry density (kg/m^3)	Water content (%)	Degree of saturation (%)	Mean compression stress (p = 800 kPa)				Maximum shear strains ($\gamma_{\theta z}$, −)		
					$K = \sigma_r/\sigma_z$	σ_z (kPa)	σ_r (kPa)	σ_θ (kPa)	Cycle 1	Cycle 2	Cycle 3
I-85	0.99	1397	30.0	84	1.00	800	800	800	0.002	0.0035	0.007
I-90	1.00	1390	32.0	89	1.00	800	800	800	0.0018	0.0036	0.0073
I-95	1.03	1369	34.0	92	1.00	800	800	800	0.0018	0.0036	0.0073
V-85	1.00	1387	30.0	83	0.50	1200	600	600	0.002	0.004	0.0075
V-90	1.00	1386	31.8	88	0.50	1200	600	600	0.002	0.004	0.008
V-95	1.03	1370	34.0	92	0.69	1020	700	700	0.004	0.008	0.016
H-85	0.99	1397	30.0	84	1.11	745	830	830	0.0018	0.0036	0.0073
H-90	1.01	1381	32.2	88	1.11	745	830	830	0.0018	0.0036	0.0073
H-95	1.00	1390	34.3	95	1.11	745	830	830	0.0018	0.0036	0.0072

Table 5
Characteristics of the tests performed in the simple shear apparatus. Shear strain rate: 0.3 %/min. Tests carried out at the EPFL.

Test	Height (mm)	Diameter (mm)	Void ratio (–)	Dry density (kg/m^3)	Water content (%)	Degree of saturation (%)	Axial stress (kPa)
SS1	20.15	50.0	0.79	1554	21.0	74	800
SS2	21.09	50.0	0.83	1518	19.2	64	1200
SS3	20.25	50.0	0.82	1530	19.6	67	1600

underdamped and when Q_0 is disabled, the amplitude gradually decreases, if $c = c_c$, the oscillator is critically damped and when Q_0 is disabled, the oscillator returns to rest without oscillating. If $c > c_c$ the oscillator returns to rest without oscillating as well, and the larger c_c, the slower damping.

The damping ratio is defined as:

$$D = \frac{c}{c_c} \tag{3}$$

Damping ratio can be obtained from the logarithmic decrement (δ) of the amplitude under free oscillations in the soil column (free vibration decay method), (ASTM D4015-15e1, 2015; Senetakis et al. 2015; Madhusudhan and Kumar, 2013).

$$\delta = \frac{2\pi D}{\sqrt{1-D^2}}; \delta = \frac{ln(A_i/A_{i+n})}{n} \tag{4}$$

where A_i is the amplitude of cycle 'i' and A_{i+n} the amplitude of cycle 'i + n' (Fig. 1). The values of δ are evaluated from accelerometer readings while the soil is freely oscillating.

If D is small,

$$D \approx \frac{\delta}{2\pi} \tag{5}$$

2.2.3. Triaxial tests (TX)

The triaxial tests TRI 1a, TRI 2a and TRI 3a were carried out at the UPC with the device described in Romero (1999) at constant deviator rate (300 Pa/s) and the rest of the tests were performed at the École Polytechnique Fédérale de Lausanne (EPFL) in the triaxial test set-up described in Favero et al. (2017) at constant axial strain rate (0.3 %/min). The strain rate was lower than 0.3 %/min in all cases (Table 3). The influence of the strain rate in shearing is discussed in Börgesson et al. (2010), where it was concluded that strain rates lower than 60 %/min do not have influence on the shear strength.

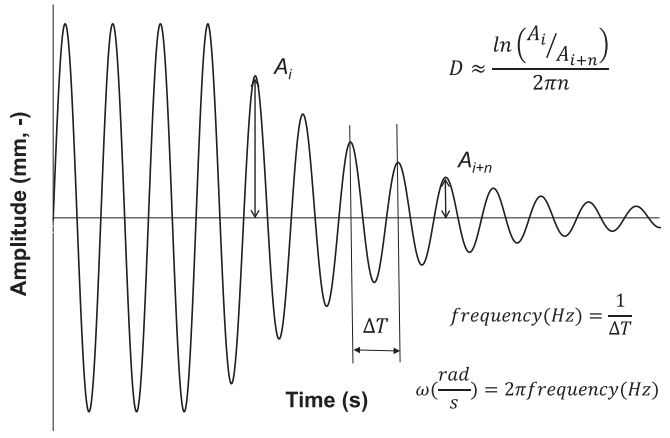

Fig. 1. Decrement of the amplitude (displacement or strain) in damping ratio measurement.

The hysteretic damping ratio in triaxial tests was calculated from stress-strain relationships with the equation (Braja and Ramana, 2011):

$$D = \frac{\Delta W}{4\pi W} \tag{6}$$

where ΔW is the total surface of a cycle unload – reload and W is the area of the triangles described in Fig. 2. Bolton and Wilson (1989) established that, once stationary loading conditions are reached, the results obtained in dry sand using the resonant column tests in dynamic and pseudo-static modes were very similar, presenting only slight differences; nevertheless, the ASTM D3999 advises that the damping ratio measured by the resonant column and by the cyclic triaxial apparatus may be different. The triaxial tests performed in this work had very small frequencies (less than 0.01 Hz with only one cycle), smaller than the range 0.1–2 Hz fixed by the ASTM D3999. Tests were carried out in unsaturated conditions, so the undrained conditions mentioned in the ASTM D3999 should be considered with caution. Iwaskari et al. (1978) also presented a study of tests in sands with resonant column and torsional shear device apparatus with hollow cylinder samples.

The shear strain used for the analysis was γ_{oct} $\left(\gamma_{oct} = \sqrt{3}\varepsilon_q\right)$, where ε_q is the distortional strain ($\varepsilon_q = \frac{2}{3}(\varepsilon_a - \varepsilon_r)$; Wood, 1990), ε_a is the axial strain and ε_r the radial strain. It was considered that all distortional strain was $\gamma_{z\theta}$, equivalent to the shear strain measured in the other tests. The shear strain considered was the amplitude of the cycles unloading–reloading. Details about the performed tests can be found in Pintado et al. (2023).

2.2.4. Hollow cylinder tests (HC)

The hollow cylinder equipment allows soil samples to be tested by controlling 4 of the 6 stress tensor components (Hight et al. 1983). These four components are σ_z, σ_r, σ_θ and $\tau_{z\theta}$. Alternatively, the stress state can be defined by the value of the three principal stresses and the direction

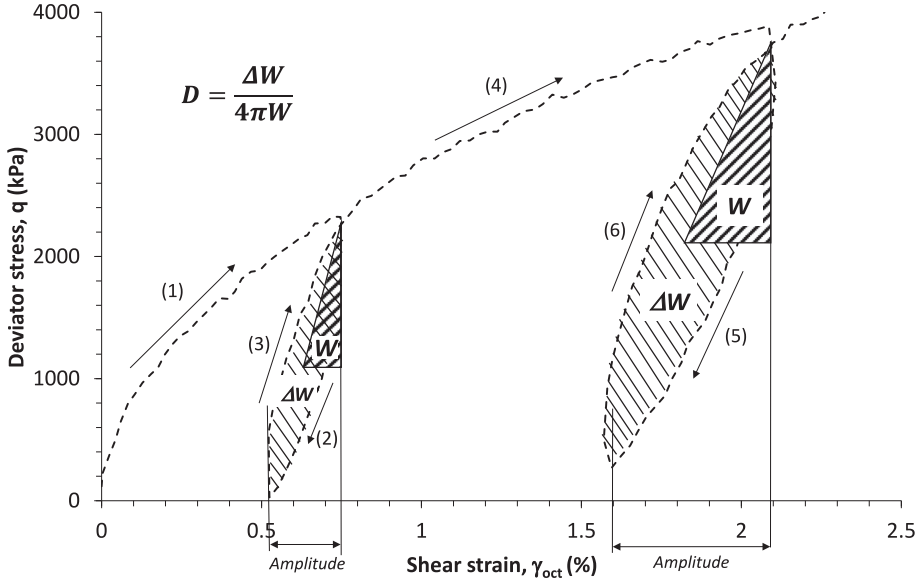

Fig. 2. Definition of the damping ratio D in triaxial tests (TRI 1b test).

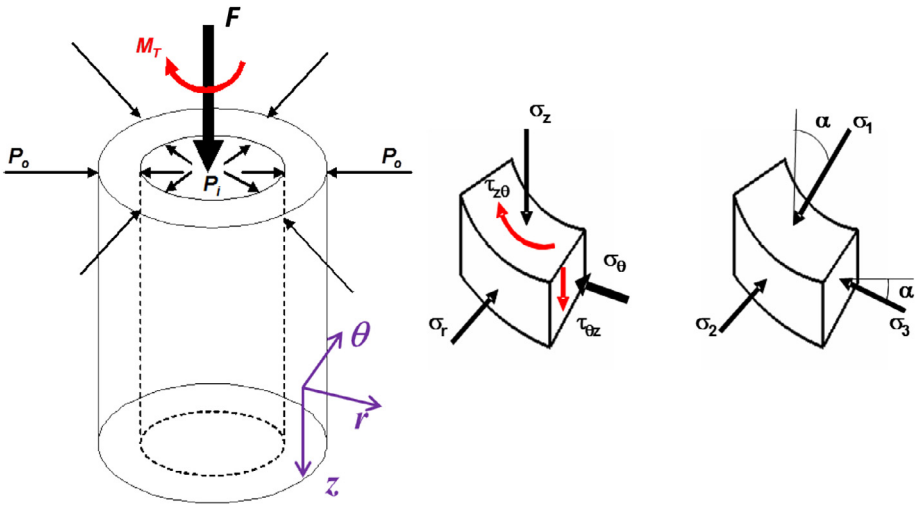

Fig. 3. Idealized stress conditions in a hollow cylinder test (after Hight et al. 1983).

of the major principal stress relative to the vertical (α), (see Fig. 3). The four stresses are applied to the hollow sample through the vertical load (F), the torsional moment (M_T) and the pressures in the external and internal chamber (Po and P_i, respectively). Strain rate was lower than 0.75 %/min in all tests.

This test has been used for the measurement of the shear properties of soils (Nishimura et al. 2007; Wrzesinski and Lechowicz, 2015). Damping ratio in cyclic strain tests can be calculated as it is shown in Fig. 4 (Lanzo and Vucetic, 1999; Nakamura et al. 2009) using the Eq. (6). All hollow cylinder tests results are presented in Weber (2019) and in Pintado et al. (2023).

2.2.5. Simple shear tests (SS)

The simple shear test equipment (Bernhardt et al. 2016; Bjerrum and Landva, 1966) only allows to control the axial or normal stress (σ_z or σ_n) and the shear stress in one direction (τ_{xz} or τ), measuring the axial strain (ε_z) and the shear strains at the shear direction (γ_{xz} or γ). The horizontal stresses σ_x and σ_y are not measured, so it is not possible to know the stress state of the sample. The simple shear stress is performed in oedometric conditions ($\varepsilon_x = \varepsilon_y = 0$). In the same way that in triaxial tests, damping ratio in cyclic strain tests can be calculated as it is shown in Fig. 5 using the Eq. (6). The shear strain considered was the amplitude of the cycles unloading–reloading.

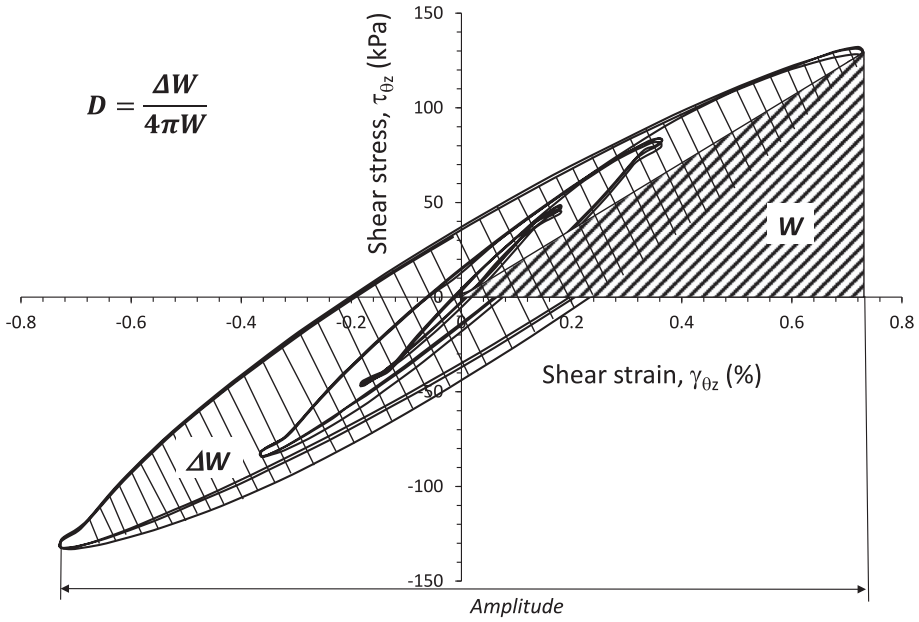

Fig. 4. Definition of the damping ratio D in hollow cylinder tests (H-85 test).

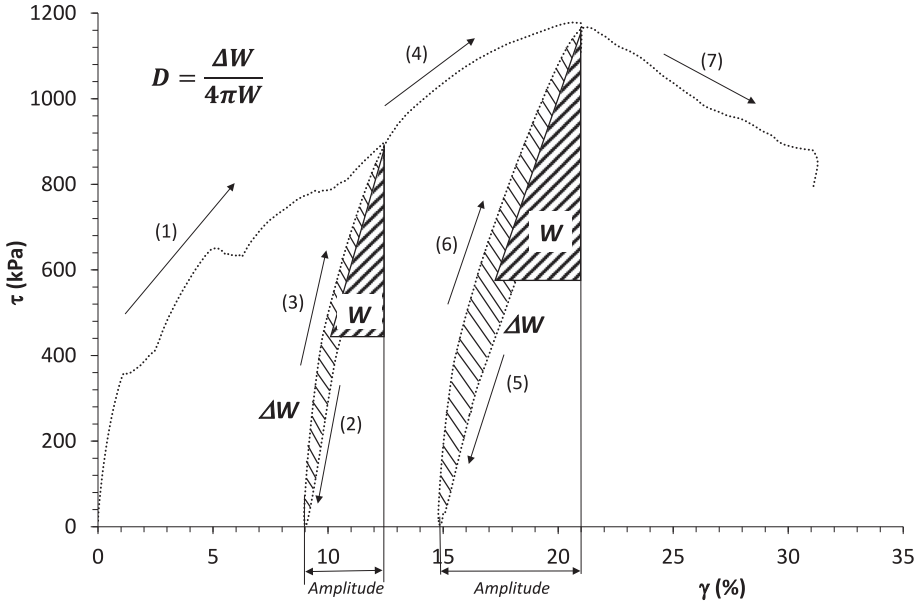

Fig. 5. Definition of the damping ratio D in simple shear tests (S3 test).

Note that the shear strain γ in this test is the same as the shear strain calculated in the resonant column test. The strain rate was 0.3 %/min. More details about these tests can be found in Pintado et al. (2023).

In triaxial and simple shear tests, the damping ratio was measured after loading the samples. During this process of loading, the samples showed elastoplastic behaviour (Fig. 2 and Fig. 5), so the damping was measured in a hardened material but in elastic regime (unloading–reloading loop). The hardening process might also happen in tests carried out in resonant column devices, but the level of strains was smaller and therefore unlikely. Tests performed in hollow cylinder might be considered in between.

3. Results

In this section, the results obtained from different techniques in Wyoming-type bentonite are presented and analysed. In addition, the results of the resonant column tests in Wyoming-type and FEBEX bentonites are compared in order to study the plasticity effect on the damping ratio. The influence of the confinement pressure, degree of satu-

Table 6
Summary of the tests carried out on compacted Wyoming-type and FEBEX bentonite samples.

Test type	Dry density (kg/m^3)	Degree of saturation (%)	Confinement pressure (kPa)	Amplitude shear strain[3)] (%)	Damping ratio (%)	Observations
Resonant column (FEBEX)	1540–1740	10–95	100–800	0.0015–0.09	0.89–4.66[4)]	–
Resonant column (Wyoming-type)	1430–1750	51–96	100–10000	0.0005–0.013	2.18–5.22[4)]	2 devices
Triaxial (Wyoming-type)	1500	22–60	1600/4000	0.20–1.21	7.1–32	2 devices. Unloading-reloading cycles
Hollow cylinder (Wyoming-type)	1400	83–95	800[1)]	0.35–3.2	2.7–33	Unloading-reloading cycles
Simple shear (Wyoming-type)	1520–1550	64–74	800–1600[2)]	2.5–6.2	8.5–10.3	Unloading-reloading cycles

[1)] Mean compression stress.
[2)] Axial stress.
[3)] Range of the shear strain amplitude in damping measurement, γ in resonant column and simple shear tests, γ_{oct} in triaxial tests and $\gamma_{\theta z}$ in hollow cylinder tests.
[4)] Measured at 800 kPa confinement pressure.

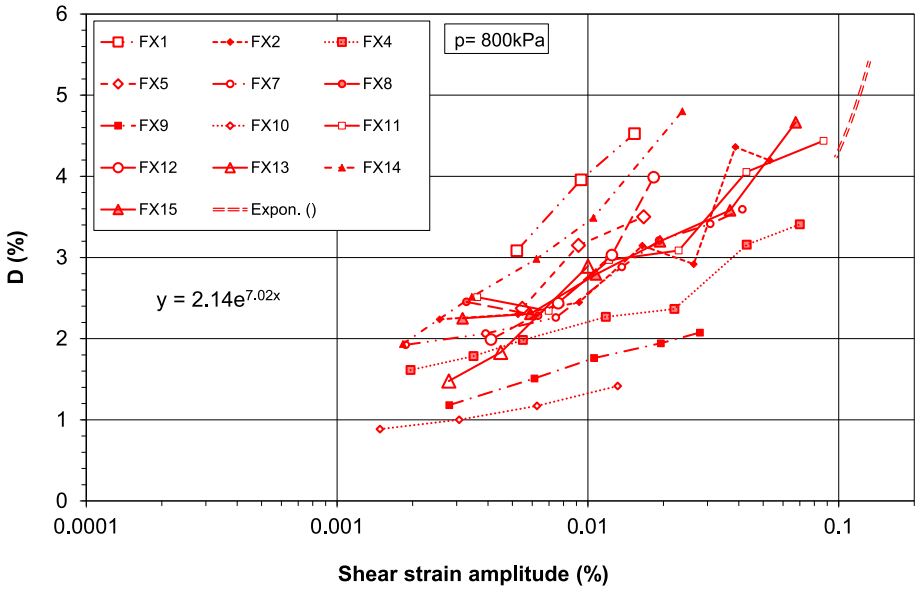

Fig. 6. Damping ratio in FEBEX bentonite. Resonant column tests with p = 800 kPa. (Table 1 indicates the name and characteristics of each test).

ration, dry density and shear strain are presented as well. Table 6 shows a summary of the tests conditions and main results. Note that the damping ratio is expressed in percentage.

3.1. Comparison between Wyoming-type and FEBEX bentonites

Wyoming-type and FEBEX are sodium and calcium bentonites with a large difference in plasticity index (PI), respectively. Wyoming-type bentonite has a PI around 450 % and FEBEX bentonite 53 %. Usually, it is assumed that the damping ratio decreases when the PI increases (Vucetic and Dobry, 1991) but it has also observed that after reaching certain PI value, the effect on the damping ratio has the opposite tendency and increases with the PI (Lanzo and Vucetic, 1999).

The resonant column tests results presented in Fig. 6 and Fig. 7 do not show significant differences in damping ratio due to the difference in PI. The shear modulus was slightly larger in Wyoming-type bentonite than in FEBEX bentonite (Pintado et al. 2019) but this statement should be taken with caution due to the large scatter observed. The caution should also be considered with the large PI of the Wyoming-type bentonite. The FEBEX bentonite is in the medium range of the PI presented by Vucetic and Dobry (1991) and the Wyoming-type bentonite is beyond the maximum PI (200 %). It is necessary to have more results of bentonites with PI between 53 % (FEBEX bentonite) and 450 % (Wyoming-type bentonite) to make conclusions about the influence of the PI in dynamic properties of bentonites.

3.2. Effect of the confinement pressure, degree of saturation and dry density on damping ratio of the Wyoming-type bentonite

Fig. 8 and Fig. 9 show the results of the resonant column tests in Wyoming-type bentonite. The increment of

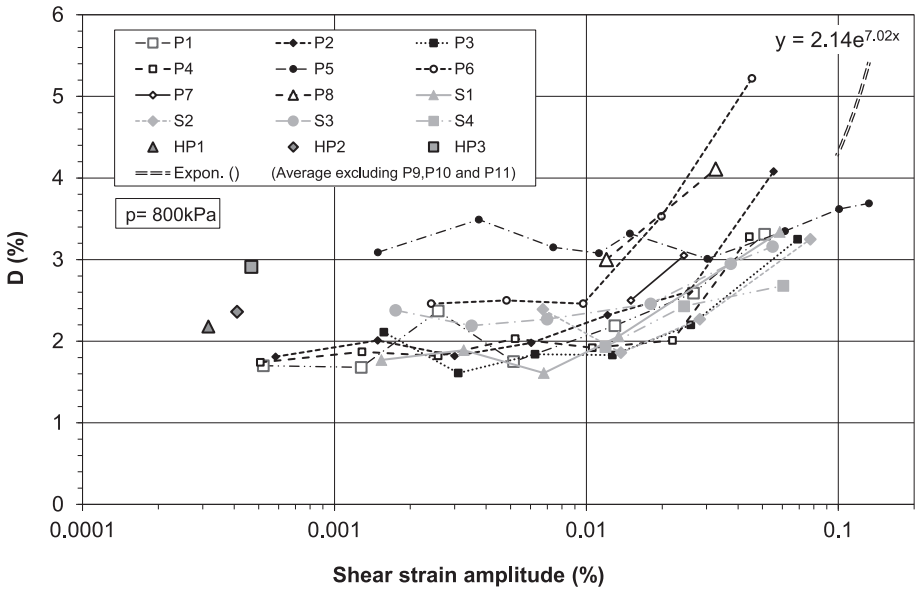

Fig. 7. Damping ratio in Wyoming-type bentonite. Resonant column tests with p = 800 kPa. (Table 1 indicates the name and characteristics of each test).

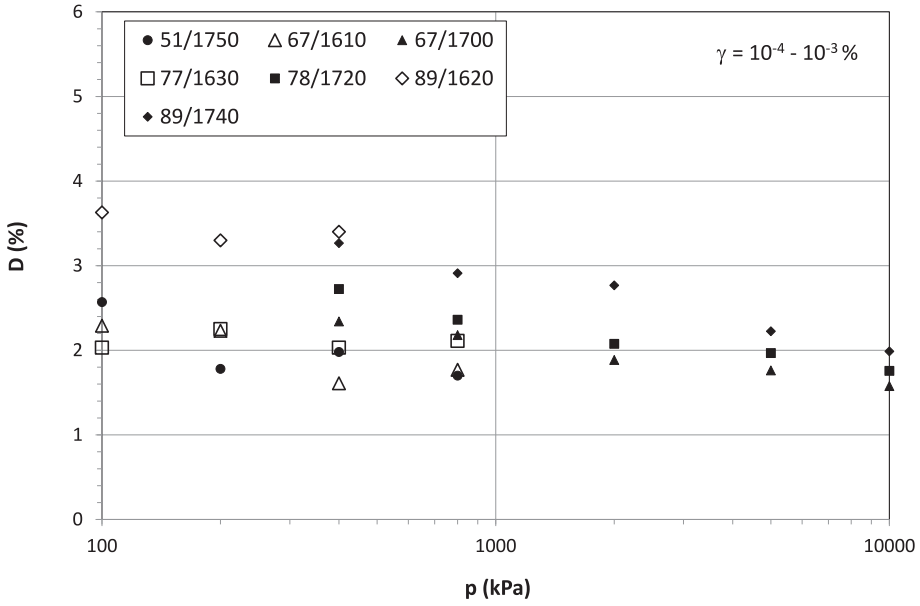

Fig. 8. Damping ratio vs confinement stress for different degrees of saturation and dry densities (Degree of saturation (%)/Dry density (kg/m^3) in the legend) in Wyoming-type bentonite.

the confinement pressure decreases the damping ratio since the larger the interparticle stress the larger the elastic domain.

It is expected that the increment of water in soils increases the damping ratio as the viscosity of water is higher than the viscosity of air (Ellis et al. 2000; Madhusudhan and Kumar, 2013; Hoyos et al. 2015). It is possible to see this increment in Fig. 8 and Fig. 9. Hence, for a given density the damping increases with degree of saturation, which is also inversely proportional to their shear stiffness as observed in Pintado et al. (2019).

It is also expected that an increment of the dry density decreases the damping ratio due to the larger stiffness and elastic domain size of the soil (see Fig. 8 and Fig. 9). It is possible to see in Fig. 8 a certain convergence of the damping ratio when the confinement stress increased. This convergence is, however, small and it was also observed in the evolution of the shear modulus with the confinement stress (Pintado et al. 2019). The degree of saturation and the dry density did not converge, so the convergence in the damping ratio observed in Fig. 8 was probably due to the increase of the confinement stress.

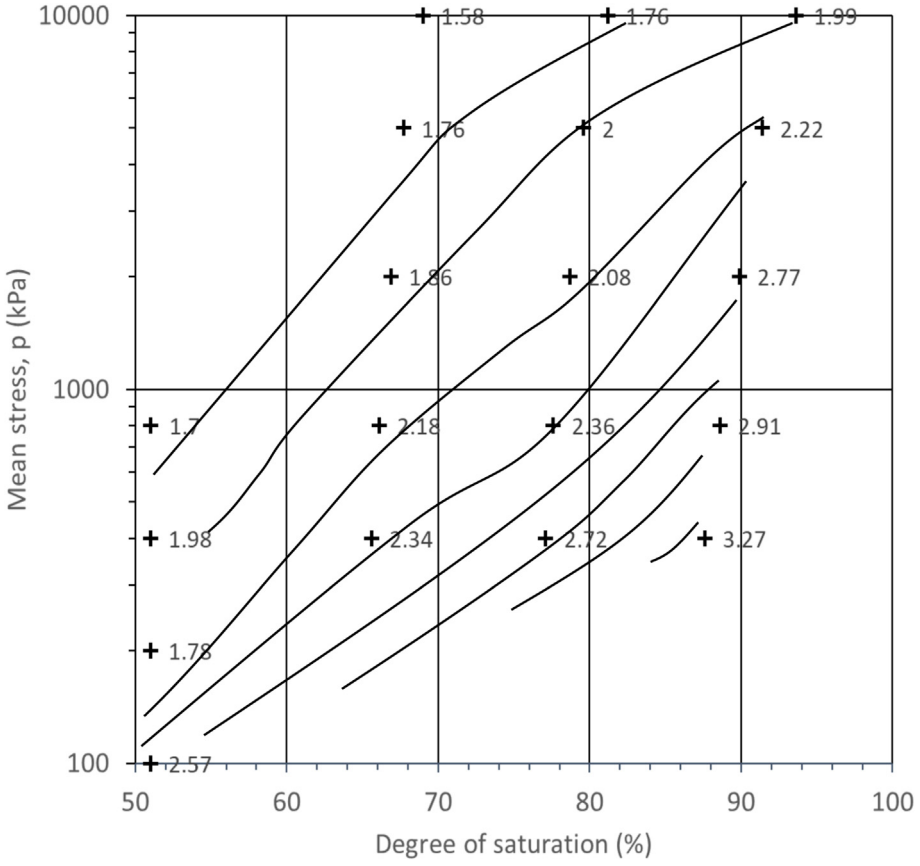

Fig. 9. Damping ratio (%) for different degrees of saturation and confinement stresses in Wyoming-type bentonite (shear strain amplitude:10^4–10^3 %).

The degree of saturation is related to the suction through the water retention curve. This relation is not unique because it depends on the density, temperature, wetting or drying path. The effect of the suction in these tests is extensively analysed in Pintado et al. (2023).

3.3. Effect of the damping ratio measurement method on the damping ratio of the Wyoming-type bentonite

Previously presented results in this section were obtained measuring the damping ratio with the resonant column device. Triaxial, hollow cylinder and simple shear tests were also carried out and the results were used for the calculation of the damping ratio. All results are presented in Fig. 10 with other results from the literature. The results show that the hollow cylinder test presents smaller values of damping ratio than the triaxial tests because the strains in hollow cylinder tests were smaller than in triaxial tests. The results follow the tendency expected by Vucetic and Dobry (1991) despite of large scatter.

Simple shear tests deformed the samples more than the triaxial and hollow cylinder tests, but the calculated damping ratios were smaller. The value of ΔW seems to be the smallest if the results presented in Fig. 2, Fig. 4 and Fig. 5 are compared.

Other tests performed in compacted bentonites are presented in Fig. 10. Balagosa et al. (2020) carried out the tests in Ca-bentonite varying the dry density from 1500 kg/m^3 to 1770 kg/m^3 and the degree of saturation between 39 % and 54 %. Tests were performed in a free-free resonant column without confinement pressure. Amini (1999) performed the tests in bentonite with a confinement pressure of 60 kPa in a resonant column under random torsional excitation conditions. Yang et al. (2020) performed the tests in Na-bentonite with a dry density of 1470 kg/m^3 and a degree of saturation of 95 % (assuming a solids density of 2750 kg/m^3). Tests were carried out in a dynamic triaxial cell test set-up with a confinement pressure of 300 kPa. The two tests from Nakamura et al. (2009) were carried out in a torsion shear test set-up, measuring almost null damping rations. The material was a mixture of Na-bentonite (70 %) and silica sand (30 %) with a dry density between 558 kg/m^3 and 679 kg/m^3 in saturated conditions and confinement pressures between 27.0 kPa and 86.2 kPa with a ratio $\frac{\sigma_{axial}}{\sigma_{radial}}$ between 1.0 and 1.3.

ASTM D3999 points out that the maximum strain level for considering non-destructive response (only elastic strains) is a shearing strain level <0.01 %. This level of strains is small and depends on the material, so it can be considered as conservative threshold. The damping ratio in triaxial and simple shear tests was measured in cycles

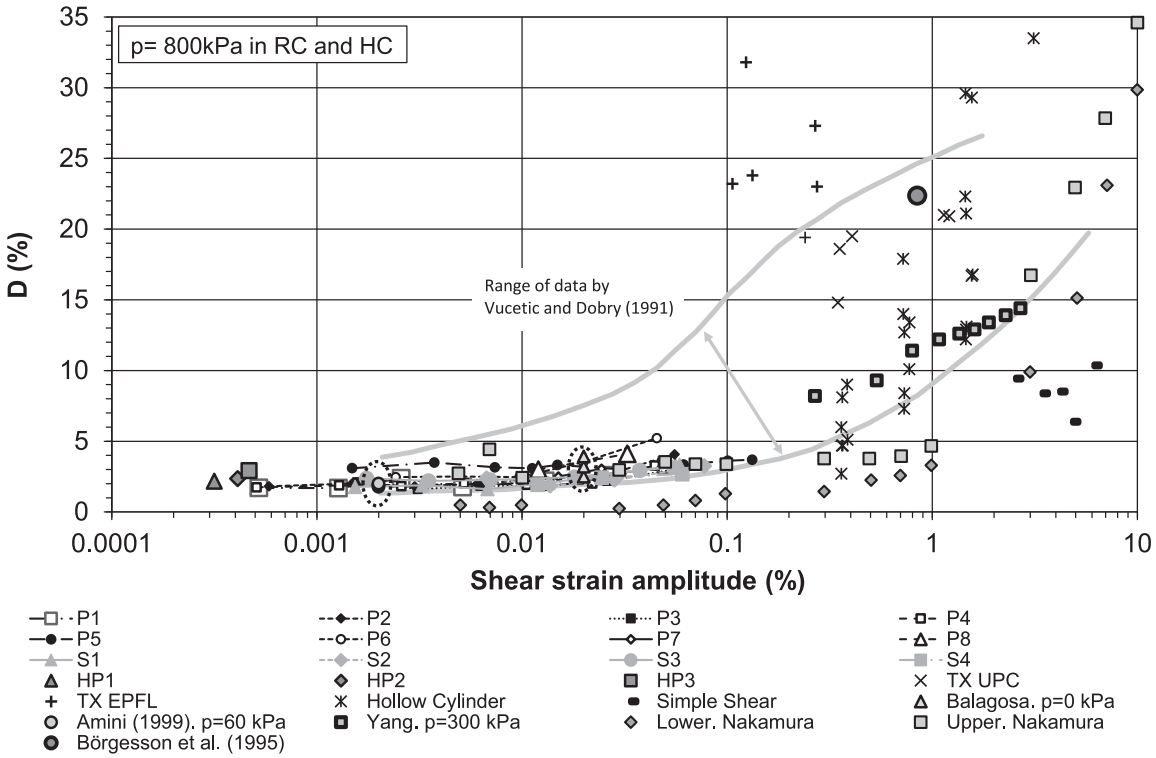

Fig. 10. Damping ratio in Wyoming-type bentonite (this work and TR-95-20, Börgesson et al. 1995) and other bentonites and a bentonite–sand mixture presented by different authors. Shear strain is γ_{oct} in triaxial tests and $\gamma_{\theta z}$ in hollow cylinder tests. Note the small values measured by Nakamura et al. (2009). Range of Vucentic and Dobry (1991) was modified for considering the amplitude.

of unloading–reloading, showing hysteretic cycle similar to cycles in hysteretic materials (Fig. 2 and Fig. 5), so it might consider elastic conditions, with the stress–strain paths inside the yield surface. Plasticity is out of the scope of this article and the movement of the yield surface during the loading paths was not studied. Plastic models of swelling materials can be found in Alonso et al. (1990); Gens and Alonso (1992); François and Laloui (2008); Navarro et al. (2014); Tachibana et al. 2020 and Ito et al. (2022) among others. The compaction pressure in hollow cylinder, triaxial and simple shear tests, which fixes the initial yield stress, was studied in Pintado et al. (2023).

Test effect of the testing apparatuses in damping ratio measurement was studied by Lanzo and Vucetic (1999) and they pointed out the discrepancies between damping ratios obtained in different tests set-ups. Khan et al. (2008) showed that the damping ratio obtained in the resonant column can be different at high level of strains depending on the test procedure, however, Hoyos et al. (2015) measured similar values of the damping ratio in resonant column tests using bender elements and the torsional mode.

It is interesting to observe in Fig. 4 the rounded borders of the hysteresis loops in hollow cylinder tests. Lanzo and Vucetic (1999) pointed out the two phenomena that cause the damping in soils: the viscosity and the nonlinearity. These authors commented that the area of a hysteresis loop will increase if the soil is either more viscous (exhibits larger creep under constant force or larger relaxation under constant deformation) or its stress–strain behaviour is more non-linear. The plasticity is associated with viscosity and bentonites have large plasticity, so the rounded borders of the hysteresis loops observed in hollow cylinder tests might be due to the viscous damping.

The two mechanisms that cause damping (viscosity and non-linearity or hysteresis) were investigated by Guido (2019). His work showed that the hysteretic damping weight decays when the damping ratio was measured with the resonant column device from the free vibration method described in ASTM D4015-15e1 (2015), so the damping ratio measured is a weighted average of both dampings, increasing the viscosity weight when the strains drop. The steady state vibration method fixes the influence of both dampings in each measurement because the maximum strain does not change.

Senetakis et al. (2015) performed a comparison between both methods, and no systematic over- or under-estimation of the observed values was observed when one method was used over the other one. The ASTM D4015-15 standard recommends both methods for the measurement of the damping ratio.

3.4. Effect of shear strain

The damping ratio remained constant till the shear strain is 0.01 % (the strain considered by the ASTM

D3999 as threshold for showing non-destructive response to the application of cyclic loading) but increased exponentially after this value. The damping ratios measured in the simple shear tests apparatus did not follow the tendency of the resonant column, hollow cylinder and triaxial tests: the damping ratios measured were smaller although the range of the strains were larger (Fig. 10 and Fig. 11). It should be noted that the dry density in simple shear tests was between the dry density of the hollow-cylinder tests and the triaxial and resonant column tests, so the reason for the lower damping ratio values in shear tests would be due to the test conditions and not due to the density differences.

3.5. Effect of water salinity

Due to the large scatter observed in this study, it cannot be concluded anything regarding the effect of water salinity on damping ratio.

3.6. Relation G/G_{max} and damping ratio

The reduction of the normalized shear modulus and the increase of the damping ratio is presented in Fig. 11 resonant column tests. In both bentonites it is possible to see an increase of the damping with the decrease of the shear modulus although in FEBEX bentonite, damping increase

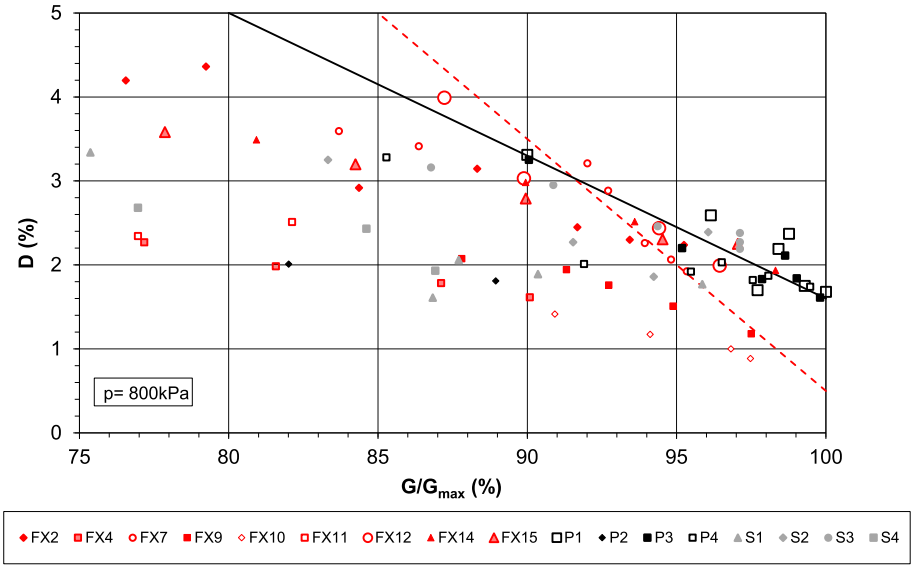

Fig. 11. Damping vs G/G_{max} in resonant column tests. Black solid and red dashed lines indicate the maximum increase of the damping ratio with G/G_{max} for Wyoming-type and FEBEX bentonites respectively.

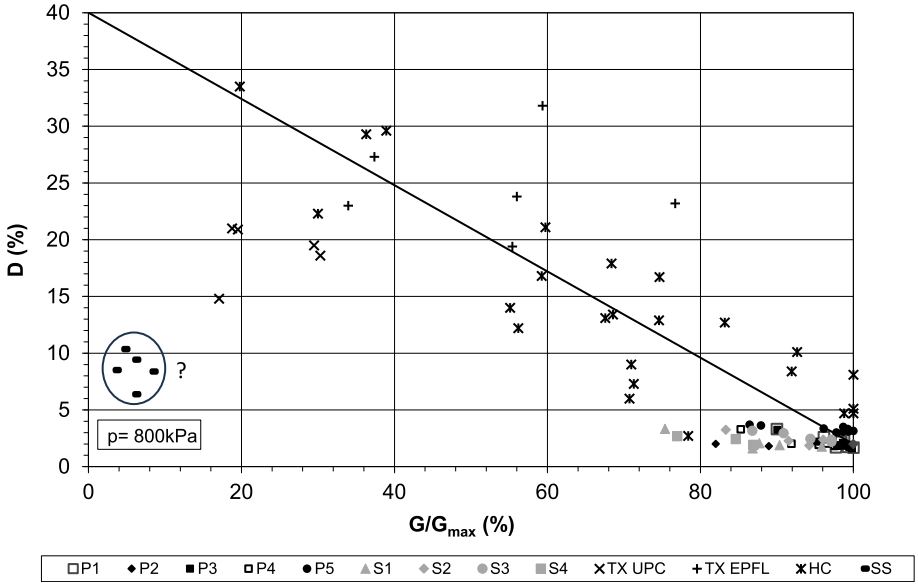

Fig. 12. Damping and G/G_{max} in performed in Wyoming-type bentonite. Solid line indicates the tendency of damping increase with G/G_{max} in hollow cylinder tests.

and shear modulus decrease is larger than in Wyoming-type bentonite.

Fig. 12 presents reduction of the normalized shear modulus and the increase of the damping ratio in the different tests carried out in Wyoming-type bentonite. In this case, the evolution in triaxial tests presents a clear difference between the tests carried out at low confinement pressure (UPC, 1600 kPa) and large confinement pressure (EPFL, 4000 kPa). The first ones seem to follow the tendency of the resonant column tests but when the confinement pressure increases, decrease of the shear modulus is larger than with lower confinement pressure. Hollow cylinder tests present large scatter and the damping ratio measured with the simple shear tests is small, as it was presented in Fig. 10. G_{max} in resonant column and in hollow cylinder tests was the maximum measured and G_{max} in triaxial and simple shear tests was estimated following the procedure described in Pintado et al. (2023) because it is not possible to measure the maximum shear modulus in these tests due to the level of strains is too high. The value of G_{max} has uncertainties and it might explain part of the scattering of the results presented in Fig. 12.

Fig. 13 presents the damping ratio and G/G_{max} versus shear strains in resonant column tests. Although the results presented large scatter, it can be observed that the reduction of the shear modulus and the increment of the damp-

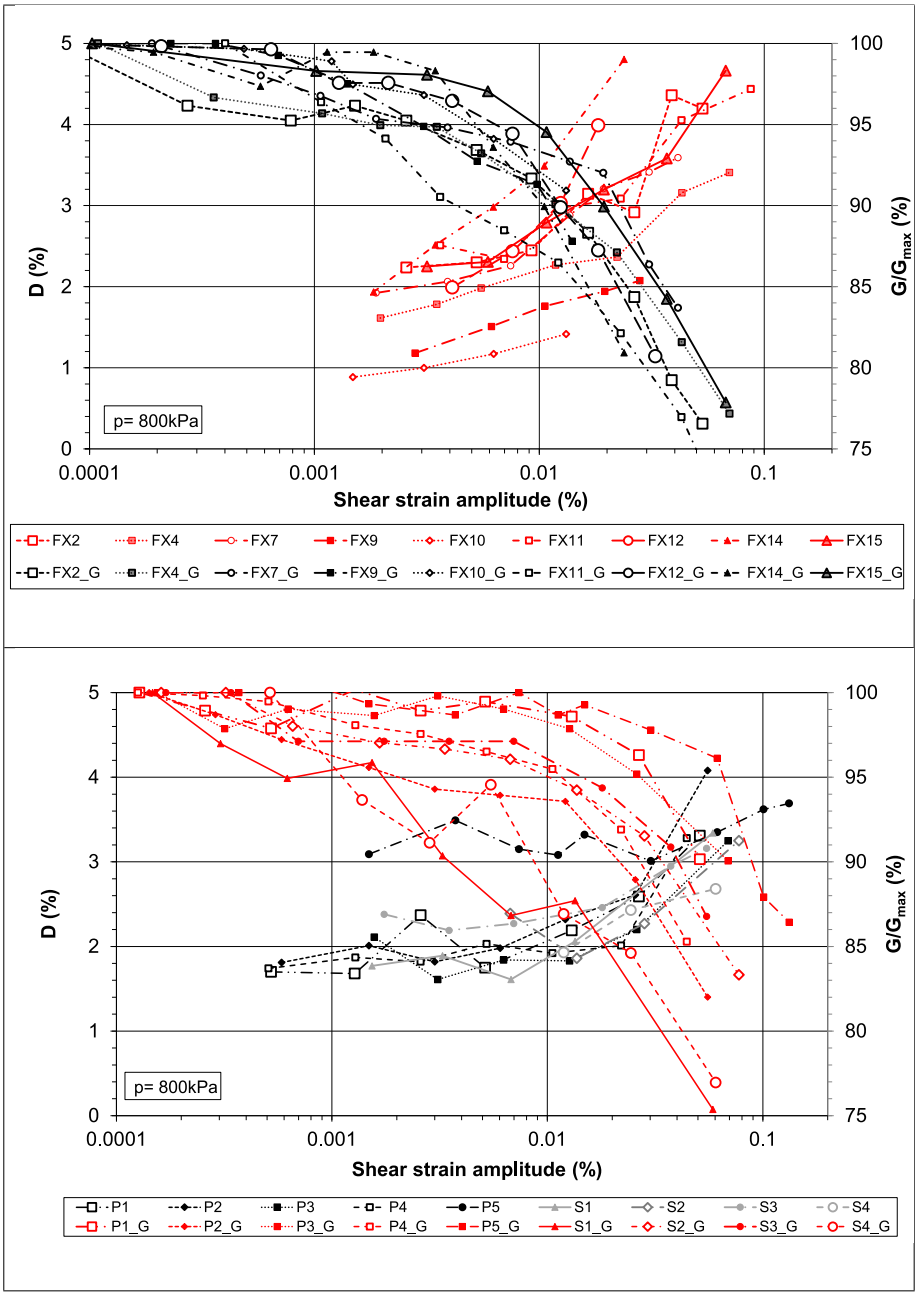

Fig. 13. Damping and G/G_{max} vs shear strains in resonant column tests performed in FEBEX bentonite (up) and Wyoming-type bentonite (down).

ing ratio start at the same range of shear strains (0.01–0.1 % in Wyoming-type bentonite and 0.001–0.01 % in FEBEX bentonite. These results are consistent with Vucetic and Dobry (1991) that predict larger shear strains for changes in shear modulus and damping ratio when the PI increases.

Other results presenting the evolution of the G/G_{max} and damping ratio vs shear strains can be found in Yang and Woods (2015) in cemented clay, Kallioglou et al. (2008) in cohesive soils, Lo Presti et al. (1997) in different soils and Kokusho et al. (1982) in soft clay.

4. Conclusions

The findings of this work can be summarized as follows:

- The damping ratio decreases with the confinement pressure and increases with the shear strain. Both tendencies are clear. The extrapolation of the tendency when the G/G_{max} approaches to one indicates a minimum damping ratio.
- The damping ratio increases with the degree of saturation and decreases with the increase of the dry density, but these tendencies are not fully clear. It can be expected that soils will be stiffer and less damping materials in unsaturated conditions than in saturated conditions due to suction effects.
- The damping ratio data on two studied bentonites in here does not reveal any dependency of damping ratio on PI that have been noted previously. However, Wyoming bentonite used is this work has a PI of 450 %, whereas previous analyses were performed in soils with PI lower than 100 %.
- The measurement method might have influence on the obtained damping ratio. The hollow cylinder test seems to follow the tendency of the resonant column tests rather than the triaxial tests. The simple shear test clearly does not follow the tendency of the other tests.
- The damping ratio measured by other authors is near the lower bound of PI except in the results obtained with a mixture of bentonite and sand, which are found below the lower bound.
- From the results obtained, the damping ratio can be measured with the resonant column in small strains and hollow cylinder test when the strains are larger. Resonant column test gives the damping due to viscosity and non-linearity when free vibration method is used and hollow cylinder test, the damping due to non-linearity. The results of triaxial and simple shear tests methods should be used with caution.
- The results from different laboratories and different apparatus concur to have a quite-unified evaluation of the studied properties, which is a good indication of the robustness of the study. Unfortunately, the results presented large scatter, partially due to the different properties (dry density and degree of saturation) of the samples tested.

CRediT authorship contribution statement

X. Pintado: Writing – review & editing, Writing – original draft, Supervision, Methodology, Investigation, Formal analysis, Data curation. **S. Kumpulainen:** Writing – review & editing, Writing – original draft, Project administration, Investigation, Data curation. **E. Romero:** Writing – original draft, Project administration, Investigation. **J. Suriol:** Investigation, Data curation. **A. Lloret:** Writing – review & editing, Writing – original draft, Project administration, Investigation. **R.C. Weber:** Investigation. **B.N. Madhusudhan:** Writing – original draft, Investigation. **A. Ferrari:** Writing – review & editing, Writing – original draft, Project administration, Investigation. **J. Kim:** Investigation, Data curation. **K. Koskinen:** Supervision, Project administration, Funding acquisition. **V. Heino:** Supervision, Project administration, Funding acquisition.

Acknowledgements

Financial support of Posiva Oy (Finland) through a collaboration agreement with Mitta Engineering Oy and CIMNE (Spain), EPFL (Switzerland) and Soton (United Kingdom) is greatly acknowledged. Authors appreciate the comments from Barbara Pastina (Posiva, Oy).

References

Alonso, E.E., Gens, A., Josa, A., 1990. A constitutive model for partially saturated soils. Géotechnique 40 (3), 405–430.

Amini, F., 1999. Effect of time on dynamic properties of cohesive soils using improved transfer function estimators. Soil Dyn. Earthq. Eng. 18 (6), 457–461.

Anderson, D.G., Stokoe, K.H., 1978. Shear modulus: A time-dependent soil property. In: Silver, M., Tiedemann, D. (Eds.), Dynamic Geotechnical Testing. ASTM International, West Conshohocken, PA, pp. 66–90.

Apted, M., Berryman, K., Chapman, N.A., Cloos, M., Connor, Ch., Katayama, K., Sparks, S., Tsuchi, H., 2004. Locating a radioactive waste repository in the Ring of Fire. Eos Trans. AGU 85 (85), 465–480.

ASTM D2216-19, 2019. Standard Test Methods for Laboratory Determination of Water (Moisture) Content of Soil and Rock by Mass, ASTM International, West Conshohocken, PA. http://www.astm.org.

ASTM D3999, 2012. Standard Test Methods for the Determination of the Modulus and Damping Properties of Soils Using the Cyclic Triaxial Apparatus, ASTM International, West Conshohocken, PA. http://www.astm.org.

ASTM D4015-15e1, 2015. Standard Test Methods for Modulus and Damping of Soils by Fixed-Base Resonant Column Devices, ASTM International, West Conshohocken, PA. http://www.astm.org.

Balagosa, J., Yoon, S., Choo, Y.W., 2020. Experimental investigation on small-strain dynamic properties and unconfined compressive strength of Gyeongju compacted bentonite for nuclear waste repository. KSCE J. Civ. Eng. 24 (9), 2657–2668.

Bernhardt, M.L., Biscontin, G., O'Sullivan, C., 2016. Experimental validation study of 3D direct simple shear DEM simulations. Soils Found. 56 (3), 336–347.

Bishop, A.W., Donald, I.B., 1961. The experimental study of party saturated soil in the triaxial apparatus. In: Proceedings of the 5th Conference on Soil Mechanics and Foundation Engineering, vol. 1, pp. 13–21.

Bjerrum, L., Landva, A., 1966. Direct simple shear tests on a Norwegian quick clay. Géotechnique 16 (1), 1–20.
Bolton, M.D., Wilson, J.M.R., 1989. An experimental and theoretical comparison between static and dynamic torsional soil tests. Géotechnique 39 (4), 585–599.
Börgesson, L., Johannesson, L.-E., Sandén, T., Hernelind, J., 1995. Modelling of the physical behaviour of water saturated clay barriers. Laboratory tests, material models and finite element application. SKB report TR 95-20. Stockholm, Sweden.
Börgesson, L., Dueck, A., Johannesson, L.-E., 2010. Material model for shear of the buffer – evaluation of laboratory test results. SKB report TR 10-31. Stockholm, Sweden.
Braja, M.D., Ramana, G.V., 2011. Principles of Soil Dynamics, second ed. Cenage, India.
Castellanos, E., Villar, M.V., Romero, E., Lloret, A., Gens, A., 2008. Chemical impact on the hydro-mechanical behaviour of high-density FEBEX bentonite. Phys. Chem. Earth, Parts A/B/C 33, S516–S526.
Ellis, E.A., Soga, K., Bransby, M.F., Sato, M., 2000. Resonant column testing of sands with different viscosity pore fluids. J. Geotech. Geoenviron. Eng. 126 (1), 10–17.
Favero, V., Ferrari, A., Laloui, L., 2017. Anisotropic behaviour of Opalinus Clay through consolidated and drained triaxial testing in saturated conditions. Rock Mech. Rock Eng. 51, 1305–1319.
François, B., Laloui, L., 2008. ACMEG-TS: a constitutive model for unsaturated soils under non-isothermal conditions. Int. J. Numer. Anal. Meth. Geomech. 32, 1955–1988.
Gens, A., Alonso, E.E., 1992. A framework for the behaviour of unsaturated expanive clays. Can. Geotech. J. 29, 1013–1032.
Guido, N., 2019. Modelización y análisis del comportamiento dinámico de suelos ensayados en la columna resonante (in Spanish). Master thesis. Universitat Politècnica de Catalunya. Barcelona, Spain.
Hight, D.W., Gens, A., Symes, M.J., 1983. The development of a new hollow cylinder apparatus for investigating the effects of principal stress rotation in soils. Géotechnique 33 (4), 355–383.
Hoyos, L.R., Suescún-Florez, E.A., Puppala, A.J., 2015. Stiffness of intermediate unsaturated soil from simultaneous suction-controlled resonant column and bender element testing. Eng. Geol. 188, 10–28.
Hung, W.-Y., Nguyen, T.A., Hsu, J.-J., Wu, Y.-C., Hsie, M.-H., 2020. Seismic response of canisters embedded in a repository analyzed through centrifuge modeling. Eng. Geol. 277 105803.
Ito, S., Tachibana, S., Takeyama, T., Iizuka, A., 2022. Constitutive model for swelling properties of unsaturated bentonite buffer materials during saturation. Soils Found. 62 101161.
Iwaskari, T., Tatsuoka, F., Takagi, Y., 1978. Shear moduli of sands under cyclic torsional shear loading. Soils Found. 18 (1), 39–56.
Kaisko, O., Malm, M., 2019. Microearthquakes during the construction and excavation of the final repository for the spent nuclear fuel at Olkiluoto in 2002–2018. Posiva Working Report 2019-05. Eurajoki, Finland.
Kallioglou, P., Tika, Th., Pitilakis, K., 2008. Shear modulus and damping ratio of cohesive soils. J. Earthq. Eng. 12, 879–913.
Karnland, O., Olsson, S., Nilsson, U., 2006. Mineralogy and sealing properties of various bentonites and smectite-rich clay materials. SKB Technical Report TR-06-30, Stockholm, Sweden.
Khan, Z.H., Casacante, M., El Naggar, M.H., Lai, C.G., 2008. Measurement of frequency-dependent dynamic properties of soils using the resonant-column device. J. Geotech. Geoenviron. Eng. 134 (9), 1319–1326.
Kiviranta, L., Kumpulainen, S., Pintado, X., Karttunen, P., Schatz, T., 2018. Characterization of bentonite and clay materials 2012–2015. Posiva Working Report 2016-05, Eurajoki, Finland.
Kokusho, T., Yoshida, Y., Esashi, Y., 1982. Dynamic properties of soft clay for wide strain range. Soils Found. 22 (4), 1–18.
Kuusisto, M., Malm, M., Kaisko. O., Rinne, L., Lahtien, S., Saaranen, V., Pirttisalo, T., 2023. Results of monitoring at Olkiluoto in 2022, Rock mechanics. Posiva Working Report 2023-04. Eurajoki, Finland.
Lanzo, G., Vucetic, M., 1999. Effect of soil plasticity on damping ratio at small cyclic strains. Soils Found. 39 (4), 131–141.
Lei, Q., Loew, S., 2021. Modelling coseismic displacements of fracture systems in crystalline rock during large earthquakes: Implications for the safety of nuclear waste repositories. Int. J. Rock Mech. Min. Sci. 138 104590.
Lo Presti, D.C.F., Jamiolkowski, M., Pallara, O., Cavallaro, A., Pedroni, S., 1997. Shear modulus and damping of soils. Géotechnique 47 (3), 603–617.
Madhusudhan, B.N., Kumar, J., 2013. Damping of sands for varying saturation. J. Geotech. Geonviron. Eng. 139 (9), 1625–1630.
Nakamura, M., Kawano, K., Thuan Thai, B., Uchimura, T., Sugo, K., Towhata, I., 2009. Preparation of water-saturated bentonite samples and their use in torsion shear tests. Soils Found. 49 (6), 981–991.
Navarro, V., Asensio, L., Yustres, A., Pintado, X., Alonso, J., 2014. An elastoplastic model of bentonites free swelling. Eng. Geol. 181, 190–201.
Nishimura, S., Minh, N.A., Jardine, R.J., 2007. Shear strength anisotropy of natural London Clay. Géotechnique 57 (1), 49–62.
NUMO, 2017. TOPAZ Project. Long-term Tectonic Hazard to Geological Repositories. NUMO report TR-16-04, Tokyo, Japan.
Peng, Y.C., 2013. Spent nuclear fuel disposal in Taiwan. Chapter in book Infrastructure Systems for Nuclear Energy. John Willey and Sons, pp. 497–502 (Print ISBN: 9781119975854).
Pintado, X., Romero, E., Suriol, J., Lloret, A., Madhusudhan, B., 2019. Small-strain shear stiffness of compacted bentonites for engineered barrier system. Geomech. Energy Environ. 18, 1–12.
Pintado, X., Kumpulainen, S., Romero, E., Lloret, A., Weber, R.C., Ferrari, A., Villar, M.V., Abed, A., Solowski, W., Heino, V., 2023. Shear strength and shear stiffness analysis of compacted Wyoming-type bentonite. Geomech. Energy Environ. 34 100468.
Posiva, 2013. Safety Case for the Disposal of Spent Nuclear Fuel at Olkiluoto. Performance Assessment 2012. Posiva Report 2012-04, Eurajoki, Finland.
Romero, E., 1999. Characterisation and Thermo-Hydromechanical Behaviour of Unsaturated Boom Clay: an Experimental Study. PhD dissertation. Universitat Politècnica de Catalunya. Barcelona, Spain.
Ruotsalainen, P., Ahokas, H., Heikkinen, E., Lindh, J., Nummela, J., 2000. Groundwater salinity at the Olkiluoto site. Posiva Working Report 2000–26. Eurajoki, Finland.
Saari, J., 2012. Seismic activity parameters of the Olkiluoto site. Posiva Report 2012-34, Eurajoki, Finland.
Senetakis, K., Anastasiadis, A., Pitilakis, K., 2015. A comparison of material damping measurements in resonant column using the steady-state and free-vibration decay methods. Soil Dyn. Earthq. Eng. 74, 10–13.
SKB, 2010. Design, production and initial state of the closure. SKB Technical Report TR-10-17, Stockholm, Sweden.
Stepp, J.C., Wong, I., Whitney, J., Abrahamson, N., Toro, G., Youngs, R., Coppersmith, K., Savy, J., Sullivan, T., 2001. Probabilistic Seismic Hazard Analyses for Ground Motions and Fault Displacement at Yucca Mountain, Nevada. Earthquake Spectra 17 (1), 113–151.
Tachibana, S., Ito, S., Iizuka, A., 2020. Constitutive model with a concept of plastic rebound for expansive soils. Soils Found. 60, 179–197.
Tang, A.M., Cui, Y.J., 2010. Effects of mineralogy on thermo-hydro-mechanical parameters of MX-80 bentonite. J. Rock Mech. Geotech. Eng. 2 (1), 91–96.
Toprak, E., Olivella, S., Pintado, X., 2020. Modelling engineered barriers for spent nuclear fuel repository using a double-structure model for pellets. Environ. Geotech. 71 (1), 72–94.
Tsai, C.C., Chang, Y.T., Ge, L., 2019. Dynamic properties of buffer materials by resonant column test. In: Proceedings of the XVII European Conference on Soil Mechanics and Geotechnical Engineering, Reykjavik, Iceland.
Villar, M.V., Lloret, A., 2001. Variation of the intrinsic permeability of expansive clays upon saturation. In: Proceedings of International symposium on Suction, Swelling, Permeability and Structure of Clays, Shizouka, Japan, pp. 259–266.
Villar, M.V., Lloret, A., 2008. Influence of dry density and water content on the swelling of a compacted bentonite. Appl. Clay Sci. 39, 38–49.

Vucetic, M., Dobry, R., 1991. Effect of soil plasticity on cyclic response. J. Geotech. Eng. 117 (1), 89–107.

Weber, R.C., 2019. Comportamiento de un suelo compactado bajo un estado generalizado de tensiones. PhD dissertation. Universitat Politècnica de Catalunya (UPC), Barcelona, Spain.

Winberry, J.P., Huerta, A.D., Anandakrishnan, S., Aster, R.C., Nyblade, A.A., Wiens, D.A., 2020. Glacial earthquakes and precursory seismicity associated with Thwaites Glacier calving. Geophys. Res. Lett. 47 (3) e2019GL086178.

Wood, D.M., 1990. Soil Behaviour and Critical State Soil Mechanics. Cambridge University Press.

Wrzesinski, G., Lechowicz, Z., 2015. Testing of undrained shear strength in a hollow cylinder apparatus. Studia Geotechnica et Mechanica 37 (2), 69–73.

Yang, Z., Cui, Y., Li, G., Liu, X., Wang, C., Shi, W., Ling, X., 2020. Effect of freeze-thaw cycles on the physical and dynamic characteristic of modified Na-bentonite by KCl. Arab. J. Geosci. 13 (23), 1–15.

Yang, L., Woods, R.D., 2015. Shear stiffness modeling of cemented clay. Can. Geotech. J. 52 (2), 156–166.